Experimental Characterization of Multitone EM Immunity of Integrated Oscillators Under Thermal Stress

Qazi Mashaal Khan, Lokesh Devaraj, Richard Perdriau, Alastair Ruddle, Tim Claeys, Mohamed Ramdani, Mohsen Koohestani

IEEE Access
Multidisciplinary | Rapid Review | Open Access Journal

Received 9 June 2022, accepted 5 August 2022, date of publication 8 August 2022, date of current version 15 August 2022.

Digital Object Identifier 10.1109/ACCESS.2022.3197659

RESEARCH ARTICLE

Experimental Characterization of Multitone EM Immunity of Integrated Oscillators Under Thermal Stress

QAZI MASHAAL KHAN[1,4], (Graduate Student Member, IEEE), LOKESH DEVARAJ[2], (Student Member, IEEE), RICHARD PERDRIAU[1,5], (Senior Member, IEEE), ALASTAIR R. RUDDLE[2], (Senior Member, IEEE), TIM CLAEYS[3], (Member, IEEE), MOHAMED RAMDANI[1,5], (Senior Member, IEEE), AND MOHSEN KOOHESTANI[1,5], (Senior Member, IEEE)

[1]Department of Electrical and Electronic Engineering, ESEO School of Engineering, 49107 Angers, France
[2]HORIBA MIRA Ltd., Nuneaton CV10 0TU, U.K.
[3]M-Group, KU Leuven Campus Brugge, 8200 Bruges, Belgium
[4]Department of Electrical Engineering, Institut National des Sciences Appliquées, 35708 Rennes, France
[5]Institute of Electronics and Telecommunications of Rennes, University of Rennes 1, 35042 Rennes, France

Corresponding author: Qazi Mashaal Khan (qazimashaal.khan@eseo.fr)

This work was supported by the European Union's Horizon 2020 Research and Innovation Program under the Marie Skłodowska-Curie under Grant 812790 (MSCA-ETN PETER). This publication reflects only the authors' view, exempting the European Union from any liability. Project website: http://etn-peter.eu/.

ABSTRACT The reliable operation of an integrated circuit can be affected by environmental changes, such as of multiple frequency electromagnetic (EM) disturbances and temperature variations. This paper compares the performance of two oscillator circuits, namely a current-starved voltage controlled oscillator and a ring oscillator integrated into a chip, in terms of their immunity to multitone direct power injection while under the influence of thermal stress. The objective is to demonstrate by the means of measurements the synergistic effect caused by multitone EM disturbances in a test chip, in contrast to the conventional single-tone EM disturbances. Moreover, the multitone immunity levels of integrated blocks with different architectures but similar functionality are analyzed at extreme temperature deviations. Bayesian networks (BN) are applied in order to visualize the probability of circuit failure due to multitone disturbances and temperature influence. Additionally, noisy-OR and improved-adaptive-recursive-noisy-OR (I-ARNOR) probabilistic models are implemented to identify the types of causal interactions (i.e. inhibition and positive causality) between multitone disturbances and to predict the probability of failure due to higher order multitone disturbances, respectively.

INDEX TERMS Integrated circuit (IC), multitone EM disturbance, Bayesian network (BN), synergistic effect, temperature deviation, noisy-OR, improved-adaptive-recursive-noisy-OR (I-ARNOR), inhibition, positive causality.

I. INTRODUCTION

Current advancements in semiconductor technologies have enabled designers to efficiently design integrated circuits (ICs) with increasingly improved performance [1]. These ICs have smaller volume, higher density, and increased switching speed, which could result in system critical electromagnetic compatibility (EMC) issues due to radiation and conduction [2], [3]. Currently, the conducted immunity of ICs to electromagnetic interference (EMI) is usually evaluated using direct power injection (DPI) of single-tone radio frequency (RF) disturbances, following the guidelines of

The associate editor coordinating the review of this manuscript and approving it for publication was Diego Bellan.

standards such as IEC 62132-4 [4]. The susceptibility profile of ICs is determined based on the minimum power level that is required at each frequency within a given RF range to cause IC malfunction [5].

Due to the uncertain nature of the EM environment, the probability of IC failure may vary depending on the frequencies of the EM disturbances, which may occur simultaneously (i.e. multitone). In order to better emulate a real world EM environment, multitone testing can be considered an integral approach to characterize the immunity of non-linear ICs and quantify the effects of inter-modulation [6].

The IEC 61000-4-3 [7] standard describes the benefits and applications of multitone testing from the point of view of reducing the overall testing duration. From a practical perspective, the major economic limitation of multitone immunity analysis is the infinite number of possible single-tone combinations that could be tested [8]. Additionally, technical challenges such as the amplifier saturation and bandwidth of the vector signal generators, limit the number of simultaneous tones. Simulation tools complemented by predictive models such as the *noisy-OR* model [9] and its descendants have been discussed in [10], [11] to overcome some of these limitations.

Over the past years, researchers have focused on characterizing the effect of single-tone EMI on specific ICs and extracting their susceptibility profiles [12], [13], [14], [15], [16]. In addition, some authors' work aim to improve the application of EM susceptibility testing methods and predict IC immunity through analytical modelling and numerical simulation [17], [18], [19], [20]. The significance of radiated and conducted multitone immunity testing in reducing the cost and testing time has been discussed in [21], [22], [23]. Recent studies have also been carried out to examine the EM susceptibility of ICs excited by different interference waveforms [24]. In [10] and [11], simulation techniques and probabilistic models have been used to characterize the combined effect of multitone interactions for a test chip. To the best of the authors' knowledge, the experimental characterization of multitone interactions at the IC level has not been investigated.

Integrated oscillators are a crucial part of mixed-signal ICs such as RF transceivers, phase-locked loops (PLL), etc., and are indeed prone to conducted EMI, which affects their performance characteristics [25]. Furthermore, faster transistor switching in the oscillator's inverter stages can significantly increase junction temperatures and degrade its functionality [26]. Stability against temperature variations and susceptibility to multitone EM disturbances need considerable attention to ensure the reliable operation of an integrated oscillator.

The analysis of the EM immunity levels of a current-starved voltage controlled oscillator (CSVCO) and a ring oscillator (RO), was previously studied for multitone threats using simulation [11]. In this paper, the existence of the three different types of multitone causal interactions has been experimentally verified for different levels of thermal stress. Furthermore, the application of probabilistic models such as the noisy-OR and the descendants of the recursive-noisy-OR (RNOR) [27], i.e., the adaptive-RNOR (ARNOR) [28], and the improved-ARNOR (I-ARNOR) [10], has been validated for the prediction of three-tone failure probability from the single and two-tone failure probability values at respective extreme conditions.

The paper is arranged as follows. Section II describes the custom designed IC and printed circuit board (PCB), as well as discussing the robustness of the oscillators to temperature variation. Section III outlines the multitone susceptibility test setup, the test procedure, and the estimation of probability of failure due to multitone EMI. The application of BN and other probabilistic models to identify the causal interactions between simultaneously occurring single-tone disturbances is discussed in Section IV. Section V presents the experimental results for single and multitone EM disturbances under extreme temperatures for both oscillators. The use of probabilistic methods to predict the probability of EM failure for higher order tones is outlined in Section VI. Finally, the conclusions of this study are presented in Section VII.

II. CASE STUDY

This section describes the design of the oscillators that were integrated into a custom IC and the design of a PCB for conducted EM immunity testing. It is then followed by the analysis of how temperature can affect the frequency of each oscillator.

A. IC DESIGN DESCRIPTION

For this analysis, two conventional three-stage oscillators, a CSVCO and RO were selected. They were integrated, among other circuits, into the 1.52 mm × 1.52 mm PETER_ESEO research die [29], which was fabricated in silicon-on-insulator (SOI) CMOS 180 nm 5 V technology through the XFAB foundry. They were designed to have matching aspect ratios and fixed output frequency values. The design and layout of both circuits was implemented using Cadence Virtuoso.

The die is surrounded by a core-limited padring that is powered by the global power supply (V_{DD}). It consists of 52 pads with P-MOS type electrostatic discharge (ESD) protection structures to both the V_{DD} and ground. Each oscillator has an isolated power supply pad (V_{DDI}) and a single separate ground, benefiting from SOI technology [30]. The output of each oscillator is connected to an analog I/O pad with a pad capacitance, and an ESD protection which will clamp the generated signals that are not within the 0 V to 5.5 V range.

Both oscillators consist of three stage inverters to generate a sinusoidal output signal. The main difference in their topology is that the CSVCO has externally biased MOSFETs that control the current provided to its delay stage. The biasing supply (V_C) is connected to those MOSFETs, to reduce the output power and maintain a wider frequency range [31]. On the contrary, for the RO, the output frequency is only dependent on the delay cell stages and the voltage supply. A buffer is added at the output stage of the RO to stabilize the generated sinusoidal signal.

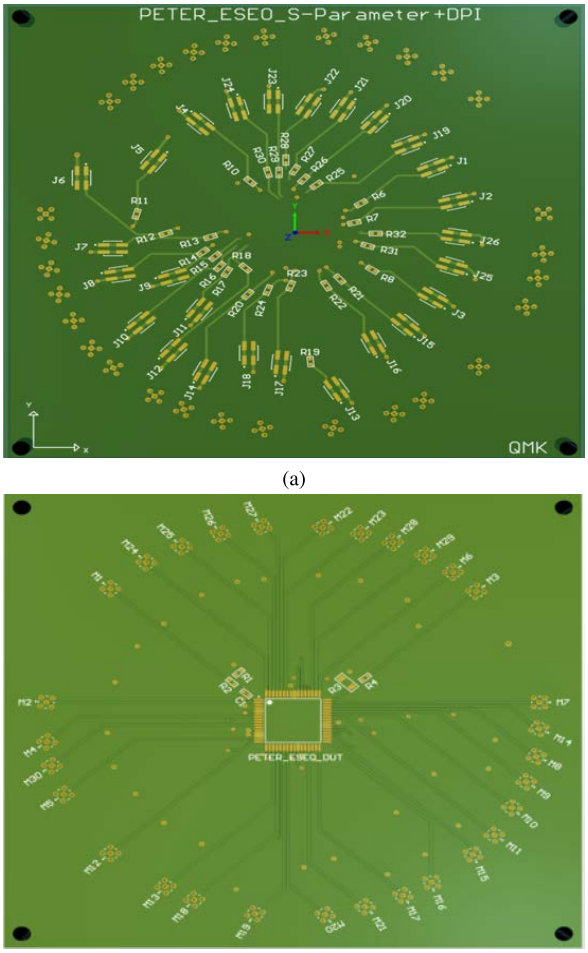

(a)

(b)

FIGURE 1. 13 cm × 13 cm 4-layer FR-4 PCB design with a total thickness of 1.6 mm: (a) top; (b) bottom. The trace length from each MMCX to the DUT pin on the bottom layer is 47 mm. The remaining two middle layers are used as ground planes. The thickness of each copper layer is 36 μm.

A 3-stage digital frequency divider (FD) circuit is added at the output stage of each oscillator to reduce the fundamental frequency of the generated signal [32]. The FD is powered by the V_{DD}, which is isolated from each oscillator's individual power supply and aids in monitoring the frequency at the analog output pin without filtering effects due to package parasitics.

The research die was packaged in a 64-pin ceramic quad flat package (CQFP). All power supply and ground pads were bonded to the package pins with spacing between them to minimize the effect of mutual inductive coupling, that makes it possible not only to inject more power into the supply pads but also monitor high frequency signals.

B. PCB DESIGN DESCRIPTION

A 13 cm × 13 cm 4-layer FR-4 PCB was designed using Altium Designer according to IEC 62132-4 [4] and manufactured through Eurocircuits as displayed in Fig 1 (a) and (b). It was made sure that the PCB does not contain non-essential circuitry (i.e. active or non-linear components) that could overload the PCB and result in uncontrolled RF behaviour [33]. This helps in measuring the immunity of the IC-under-test only. All the isolated grounds of the IC were connected to the global ground.

The bottom layer of the PCB includes the IC mounted in the middle and several micro-miniature coaxial (MMCX) through-hole female connectors to provide RF injection with a characteristic impedance of 50 Ω covering a frequency range from DC to 6 GHz (Fig. 1(b)). The reason to use MMCX instead of the standard SMA connectors is due to their smaller size, which makes it possible to test all IC pins on the same PCB. The injection paths on the bottom layer were placed radially in a circle to keep the distance between the MMCX & the pin under test equal for all pins. They were implemented as grounded co-planar wave-guides (GCPW); the latter being the variation of the CPW trace, which is usually preferred to a microstrip (MS) trace due to the field confinement inside the PCB substrate [34], [35], was selected to minimize the mutual coupling between the RF connectors as well as the components in different layers.

As shown in Fig. 1 (a), the top layer is mounted with multiple RF decoupling networks comprising a surface mount 4-pin male connector and a 470 Ω resistor in series. The resistor limits high power RF signals from being re-injected into the IC or the oscilloscope. The connectors are routed to the IC pin through MS and signal vias. The middle two layers serve as a ground plane for the MS and the GCPW on the top and bottom layers, respectively.

C. EFFECT OF TEMPERATURE VARIATION ON THE INTEGRATED OSCILLATORS

Temperature variations can increasingly affect the performance of CMOS based circuits such as oscillators. It can affect the transconductance, mobility and the threshold voltage of the CMOS transistors in the oscillator inverter stage [36]. The device under test (DUT), (i.e. the IC integrated on the PCB) is placed in a climatic chamber (Weiss Technik WK180/40) with voltage biasing applied through high temperature cables (Amphenol-RF 095-902-466-004).

While maintaining the nominal temperature for the DUT at 25 °C, the output frequency of each oscillator at the output pin (after the FD) was monitored through an oscilloscope with 1 MΩ input impedance. To see the dependence of the output frequency on temperature, the latter was increased from −40 °C to 120 °C with 5 °C step size and an accuracy of ±1 °C. Although the IC developed in SOI can withstand temperatures up to 175 °C compared to the conventional bulk CMOS technology [37], the mentioned range was selected as it complies with the temperature limit of all the components soldered on the PCB.

The variation of the output frequency with temperature for the CSVCO and the RO are shown in Fig. 2. For both oscillators the output frequency is inversely proportional to temperature. The reason for this change in frequency is due to the reduction of the mobility and the drain currents of the MOSFETs in the inverter stage with rise in temperature [25].

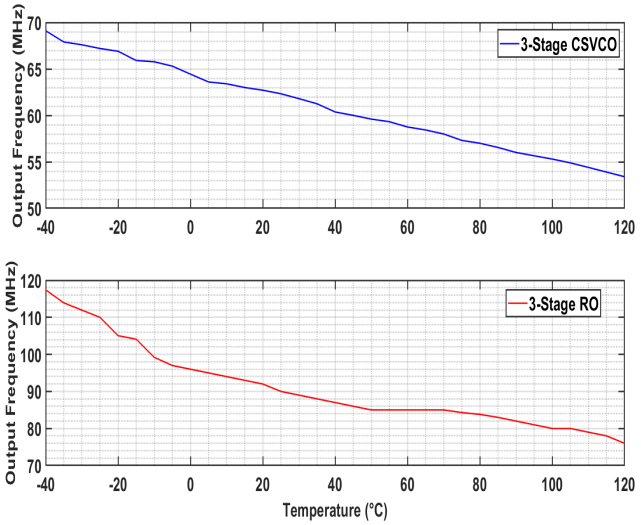

FIGURE 2. Measured frequency deviation as a function of temperature for the CSVCO and RO.

TABLE 1. Measured output frequencies of the CSVCO & RO at nominal and extreme temperatures.

Type of Oscillator	Operating frequency	Output frequency (−40 °C)	Output frequency (25 °C)	Output frequency (120 °C)
CSVCO	703 MHz	68.3 MHz	62.5 MHz	53.8 MHz
RO	955 MHz	117.4 MHz	97.7 MHz	78.2 MHz

The output frequencies for both oscillators (after the 3-stage FD) at the output pins were recorded at nominal and extreme temperatures as seen in Table 1. It was observed that the deviation of output frequency from the nominal frequency for the CSVCO and RO over the entire temperature range was ±11.68% & ±20.06%, respectively. Subsequently, it is deduced that the output frequency of CSVCO is more resilient to change in temperature compared to the RO. In the upcoming sections it will be explained how the multi-tone EM immunity of each oscillator can vary at extreme temperatures.

III. MATERIALS AND METHODS

This section introduces the hardware setup employed for multitone testing and proposes a generic multitone test procedure. The relevant failure criterion along with its application to calculate the probability of EMI failure is further explained.

A. MULTITONE TEST SETUP DESCRIPTION

The EM susceptibility experiment test bench includes a vector signal generator (R&S SMM100A), a signal & spectrum analyzer (R&S FSVA3044), a tracking DC regulated power supply (KEYSIGHT E36313A), a bias-tee (ZFBT-6GW+), an oscilloscope (R&S RTM3004), and a climatic chamber (Weiss Technik WK180/40). The setup is depicted in Fig. 3 (a). The vector signal generator was set in the arbitrary function mode, and was able to generate high order multitone signals. The signal and spectrum analyzer was used to monitor the generated multitone signal in the frequency domain. The multitone disturbance was superimposed over

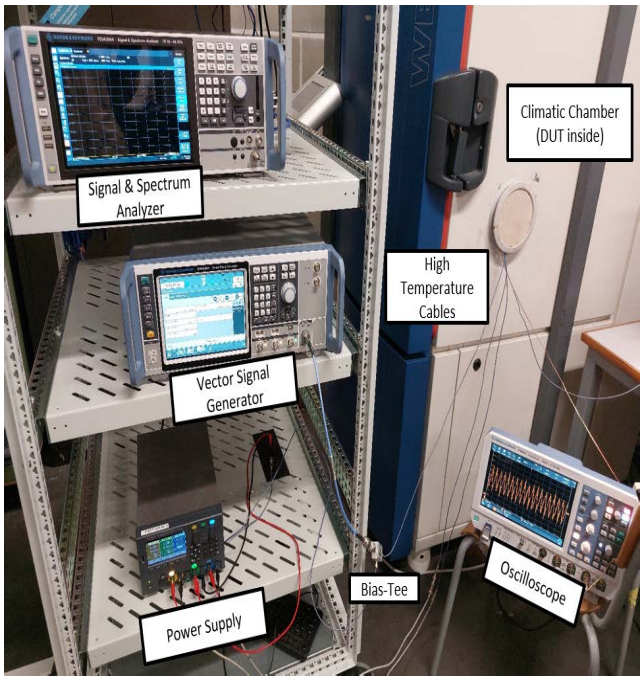

(a)

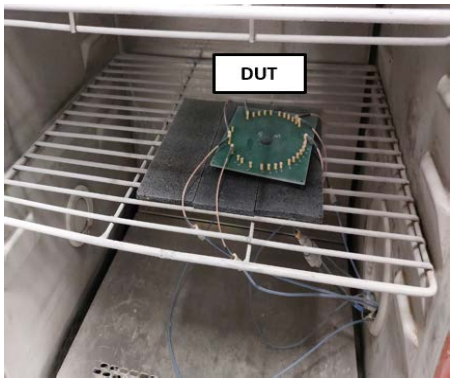

(b)

FIGURE 3. Multitone experiment (a) test setup (b) DUT inside climatic chamber.

the 5 V provided by one of the DC power supply channels via a bias-tee into the V_{DDI} pin of each oscillator. The remaining two channels of the power supply were connected to the V_{DD} and V_C pins of the DUT with a constant voltage of 5 V and 1.8 V, respectively. The V_{DD} is the global supply which powers the padring and the FD circuits in the IC. Both V_{DD} and V_C supplies were completely isolated from the injected EM disturbances. The DUT was placed inside the climatic chamber (Fig. 3 (b)) and the output pin of the tested oscillator was connected to the oscilloscope through 50 Ω high temperature cables.

One, two and three tone EM disturbances were injected into the DUT with an initial phase randomly selected between −180° to 180°. The output of each oscillator was monitored, for the input EM disturbances having the same random phase, at ambient and at extreme temperatures. The oscillators under study were susceptible to single-tone EM disturbances from

100 MHz to 1 GHz [29]. Within this range a total of 10 single-tone EMI frequencies were selected with a step size of 100 MHz. The number of frequencies selected for multitone analysis were restricted in order to limit the computational and test time. The maximum clock frequency of the vector signal generator is 44 GHz but the bandwidth for generating multitone EM disturbances, was limited to 600 MHz. Hence, to cover the entire bandwidth under test, two sets of multitone EM frequencies were chosen, which were S_1 = [100 MHz to 600 MHz] & S_2 = [500 MHz to 1 GHz]. The total number of conditional probability distribution (CPD) entries required for n frequencies is 2^n. Furthermore, the total number of non-repeating combinations for multitones up to order r is given by $C(n, r)$ [11].

A total of 29 two-tone and 40 three-tone cases were obtained from combinations of the 10 selected frequencies as shown in Table 3 (see Section VI). All combinations of EM disturbances were applied to each oscillator independently at temperatures of −40 °C, 25 °C, and 120 °C. The injected power of each tone was kept constant at 10 dBm to limit the overall combinations of multi-tones. The selected power was the minimum level at which both oscillators exhibited an observable change in the frequency of the output signal.

B. TEST PROCEDURE

This section proposes a realistic and generic test procedure for the multitone EM susceptibility analysis. The flowchart is presented in Fig. 4. Prior to initiating the multitone test, it has to be checked that the DUT is operating under nominal conditions and generating a stable output signal. The procedure steps are the following:

1) Choose the number of single-tone EM frequency samples within the susceptibility range of the DUT and assign a power step in dBm.
2) Select the injected power assigned to each single-tone EM disturbance sample.
3) Select the number of multitone EM disturbances (e.g. 2 / 3 / 4 etc.) to be applied to the DUT.
4) Generate the mutlitone EM disturbance combinations according to $C(n, r)$.
5) Select the dwell time in which the output signal stabilizes and then inject the multitone EM disturbance into the specific supply or I/O pin.
6) Monitor & record the specific parameters of the output signal (i.e. frequency, DC offset, peak-to-peak voltage etc.) and compare it with the relevant failure criterion.
7) Increase the number of combinations of multitone EM disturbances. If all combinations are assessed, then go to the next step.
8) Increment the power level of all the single-tone EM disturbances. Restart the process until the maximum power is reached.
9) At maximum power limit, save all input frequencies and output signal parameters & end the test.

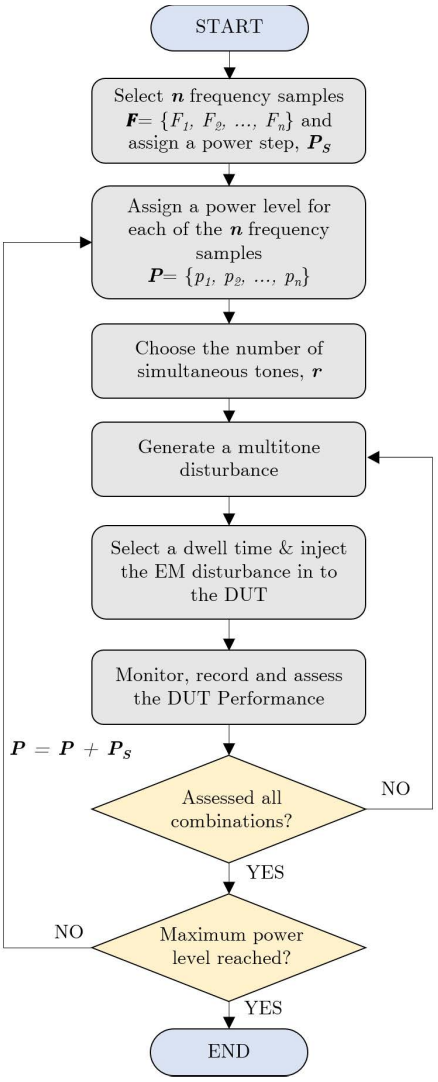

FIGURE 4. Flowchart of the single-tone (r = 1) and multitone (r > 1) immunity test procedure.

C. APPLICATION OF FAILURE CRITERION ON MULTITONE MEASUREMENTS

The operating frequency of an oscillator is conventionally used to evaluate its performance with respect to the injection of single-tone EM disturbances [38]. However, stability parameters such as the peak-to-peak voltage and the mean DC offset could also be used to characterize the conducted immunity of oscillators [39]. In this paper, to determine the performance of each circuit, the frequency observed at the output pin was monitored while being subjected to single and multitone EM disturbances under the influence of thermal stress. The failure criterion is the relative frequency deviation of ±5% from the nominal output frequencies of the CSVCO & RO, at nominal and extreme temperatures (Table 1). The tolerance limit is similar to industrial standards, which helps in characterizing the immunity of a VCO due to fluctuations in supply voltage [40].

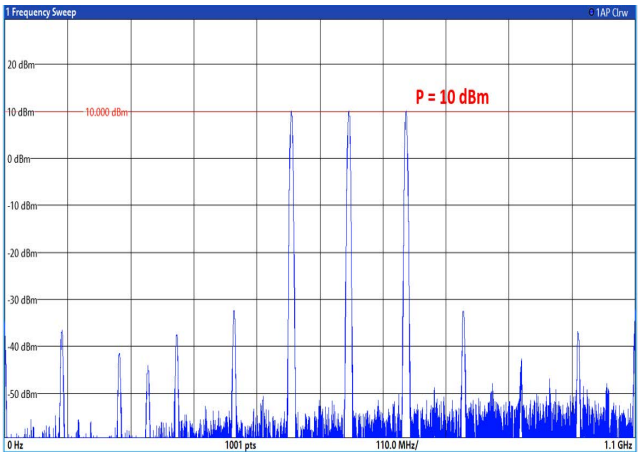

FIGURE 5. Three-tone input spectrum with injected power of 10 dBm at frequency [500, 600, 700 MHz].

All the EMI measurements were recorded for a time-period of 6 μs. A dwell time of 30 s was selected as the duration between two consecutive injected EM disturbances. That makes it possible for the tested oscillator to stabilize and reach its nominal operating frequency. The fast Fourier transform (FFT) was applied to measure the output frequency of the oscillators at discrete time steps (window size of 40 ns) over the steady-state period (6 μs).

In [11], it was demonstrated that the output response of each oscillator was different for the same injected EM disturbance. To illustrate how multitone EM disturbance can vary the output frequency of the CSVCO & RO, different cases were considered. For example, Fig. 5 displays the input frequency spectrum of the three-tone EM disturbance at 500 MHz, 600 MHz, and 700 MHz injected into the V_{DDI} pin of the DUT. The vector signal generator was connected to the signal and spectrum analyzer to observe this specific waveform. It was verified that the injected power level of each tone was constant at 10 dBm by taking into account the 1.5 dB attenuation caused by the high temperature cables. Other peaks, due to intermodulation within the generator, were also observed in the input spectrum but were considered negligible since their power levels were less than -30 dBm.

Fig. 6 (a) shows the measured output response in the frequency domain of the CSVCO at 25 °C. It corresponds to the same input frequency spectrum as observed in Fig. 5. It is clearly seen that the highest frequency peak was shifted to 59.2 MHz from the nominal frequency of the CSVCO which is 62.5 MHz. The injected three-tone EM disturbances were observed at 500 MHz, 600 MHz, and 700 MHz but with power levels lower than that of the nominal frequency of 59.2 MHz. To apply the failure criterion, the frequency with the highest individual power was considered as the true shift in frequency for all tests. In this case, the CSVCO does not fail as the output frequency is still within the tolerance limit of $\pm 5\%$. Moreover, other inter-modulating frequencies were also observed in the output spectrum but with negligible power levels.

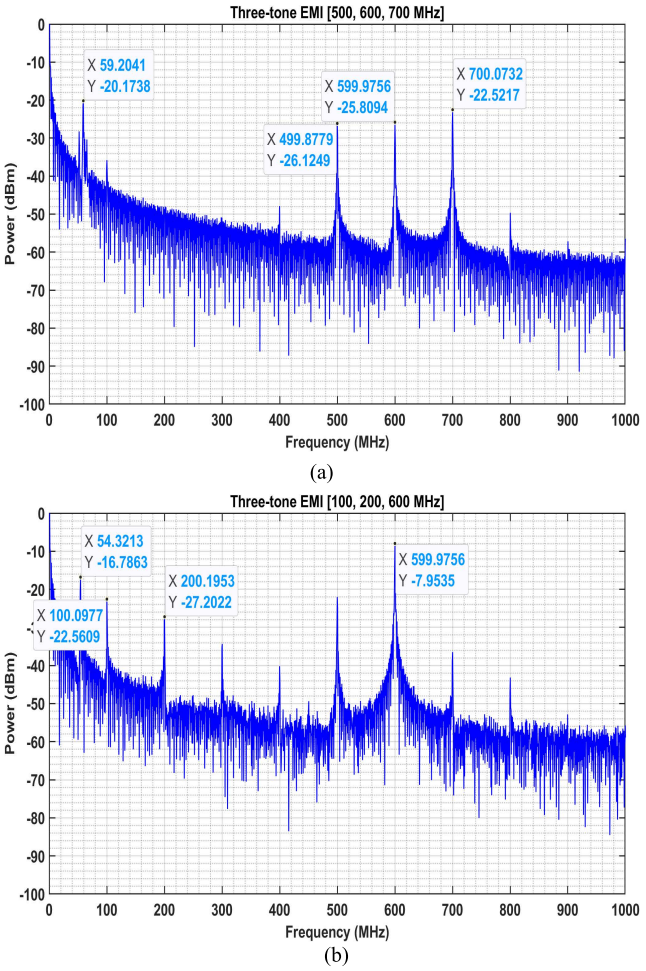

FIGURE 6. Measured output frequency of the CSVCO at 25 °C due to three-tone EM disturbance (a) [500, 600, 700 MHz]; (b) [100, 200, 600 MHz].

Another example displays the output spectrum of the CSVCO with a three-tone EM disturbance of 100 MHz, 200 MHz and 600 MHz (Fig. 6 (b)). In this case, the nominal frequency was shifted to 54.32 MHz and was outside the tolerance limit of $\pm 5\%$, thus, resulting in the CSVCO failure due to EMI. However, it was noted that the power level of 600 MHz is higher than that of 54.32 MHz by 8.83 dB. Hence, the output frequency is being locked to one of the frequencies of the injected multitone EM disturbance making the CSVCO very susceptible. Although in both cases the circuit is failing, the latter case shows the true shift in frequency from which the probability of failure can be acquired. Interestingly, it is observed that inter-modulating frequency of 500 MHz has a higher power than the remaining two (100 MHz & 200 MHz) injected EM disturbances. This is due to the injected EM disturbances being out of phase and cancelling each other.

The failure criterion is applied for each time-step in the steady state period, allowing the probability of EMI failure to be calculated by dividing the number of time steps with failure by the total number of time steps. For

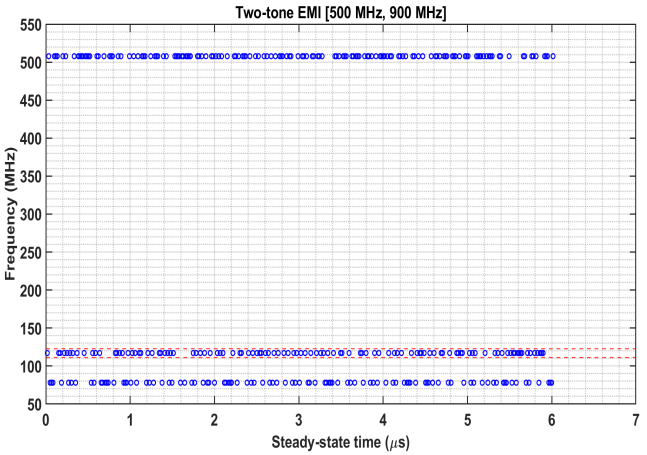

FIGURE 7. Steady-state output frequency of the RO at −40 °C, for two-tone EM disturbance [500, 900 MHz] (probability of failure = 0.6955).

example, the failures due to two-tone EM disturbance at 500 MHz and 900 MHz are visualized in Fig. 7 for the RO at −40 °C, where the dashed lines represent the ±5 % tolerance. In this case, the output frequency under EMI is found to be beyond the tolerance at several instances from the nominal frequency of 117.4 MHz. Hence, the probability of EMI failure using the measurement data, P_M is calculated as 0.6955.

IV. APPLICATION OF BAYESIAN NETWORK

The use of a probabilistic graphical model called Bayesian network (BN) has been discussed for two main purposes in this paper, which are:

1) to facilitate the probability estimation of an IC failure due to EMI, when being operated in its system environment at a given temperature;
2) to be able to predict the probability of EMI failure due to the untested combinations of multitone disturbances.

The former can be achieved by combining the following probability values:

- $P(F)$: the probability of an *EM disturbance* (F), occurring in the system environment. Where, **F** is a set consisting of n different single-tones, $\{F_1, F_2, \ldots, F_n\}$ that can occur in the system environment;
- $P(T)$: the probability of the *operating temperature* (T);
- $P(E|\ F, T)$: the conditional probability of *EMI failure* (E) due to a given EM disturbance at a given operating temperature.

The graphical representation of a generic BN model that can be applied to combine the above probability entries is discussed in Section IV. A. Further, for a simple example, first, the conditional probability of EMI failure due to two-tone disturbance is predicted from single-tone failure probabilities, then, using the estimated CPD value the probability query of an IC failure due to a specific two-tone EM disturbance at a given temperature in its system environment is estimated in Section IV. B.

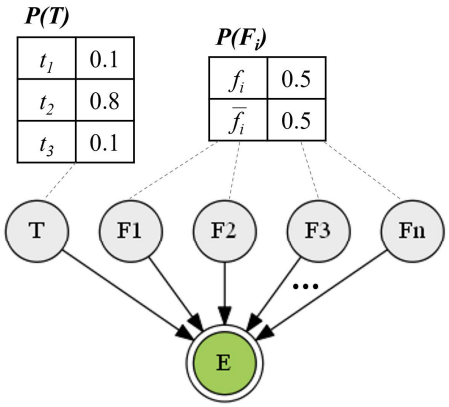

FIGURE 8. Bayesian network structure to map the influence of temperature and the causal effect of multitone EM disturbances on IC failure.

A. GRAPHICAL REPRESENTATION

In the BN shown in Fig. 8, $\{F, T, E\}$ are considered as node variables. Such that, T is assumed to have three possible states $\{t_1, t_2, t_3\}$ corresponding to operating temperatures $\{-40\ °C, 25\ °C, 120\ °C\}$. For each node variable $F_i \in F$ (where $i = 1$ to n), two possible states $\{f_i, \bar{f}_i\}$ are assumed, that denote their occurrence, i.e., present or absent respectively. Similarly, the node variable E is also considered to have two-states $\{e, \bar{e}\}$ that correspond to failure and no failure, respectively.

The directed edges in the BN depict the causal influence, i.e., from temperature and the EM disturbances on the IC failure using the directed edges $T \rightarrow E$, and $F_i \rightarrow E$, for $F_i \in F$. Hence, by using the chain rule [41], the factorization for the joint probability distribution of the variables in the BN, which is also the probability of IC failing due to EMI in its system environment, is given by:

$$P(E,\ F, T) = P(E|\ F, T) \times P(T) \times \prod_{F_i \in F} P(F_i) \qquad (1)$$

However, in order to answer all possible probability queries using (1), the BN needs to be complete. This is the case only if each node variable is assigned with a CPD table that consists of probability entries corresponding to each variable state conditioned on the Cartesian product of the states of its parent node variables (i.e., the nodes from which directed edges originate). Hence, the CPD table of the node variable E has to be filled with $3^1 \times 2^{10} = 3072$ conditional probability entries. However, as already mentioned in Section III. A, the probability entries corresponding to just 79 combinations (10 single-tones, 29 two-tones and 40 three-tones) of the total 2^{10} multitone combinations are known for all three temperature states. To account for the missing entries, the use of deterministic CPD functions introduced in [10] will be discussed further in Section IV. B. The use of a deterministic CPD function for node E in the BN is denoted by a double-line notation in Fig. 8.

Remaining node variables of the BN, i.e., T and F do not have any parents (i.e., the nodes having no incoming directed edges), hence, the CPD table for each node reduces

to a marginal probability distribution (MPD) as shown in Fig. 8. It should be noted from the probability distribution of node T, that a higher probability value is assumed for the IC operating in the ambient temperature, when compared to the extreme temperatures. This is based on the assumption that the temperature of the target system environment is mostly ambient and rarely extreme. On the other hand, the MPDs of all node variables in set **F** are considered uniform, based on the assumption that the EM disturbances with frequencies corresponding to variables in **F** occurring in the target system environment are usually unknown. Nevertheless, the CPDs for T and F can be provided by collecting statistical data or by simply relying on expert knowledge of the system.

B. DETERMINISTIC CPD FUNCTIONS

When a BN is used to map multiple causes of a single effect (like the BN shown in Fig. 8), the number of probability entries required to complete the CPD table increases exponentially with the number of parent nodes. The elicitation of such large number of conditional probability entries could become impracticable for many real-world applications, including the current investigation of estimating the IC failure probability due to multitone EM disturbances.

To avoid the exhaustive elicitation of probability entries in the CPD table for E, deterministic functions for the conditional probabilities $P(E|\ T,\ F)$ can be used [10]. The description of three different deterministic CPD functions, namely the noisy-OR, which is based on causal independence assumptions between multiple causes [27], [41], and its descendants the ARNOR and the I-ARNOR, which inherit the noisy-OR model and any known dependence information to estimate the CPD entries, is provided in [10]. Including the influence of T, the probability of an IC failure due to the multitone disturbance can be estimated using the noisy-OR CPD expression as:

$$P_N(e|\tilde{f},T) = 1 - \{(1-\lambda_0) \prod_{F_i=f_i\in\tilde{f}} (1 - P_M(e|f_i,T))\} \quad (2)$$

where e is simply the evidence of failure, i.e., $E = e$, $\tilde{f}$ indicates the assignment of a respective state for each of the n variables in set **F**, e.g., if $n = 5$, then for a three-tone disturbance $\{F_1, F_2, F_4\}$, $\tilde{f} = \{f_1, f_2, \bar{f}_3, f_4, \bar{f}_5\}$. As a shorthand, for rest of this paper, only the frequencies that are present (i.e., $F_i = f_i$) are included in $\tilde{f}$. So, for the previous example, $\tilde{f} = \{f_1, f_2, f_4\}$. In (2), $P_M(e|\ F_i, T)$ are the failure probabilities for single-tone EMI obtained from measurements and λ_0 represents the probability of failure in the absence of EMI (assumed to be zero).

Ideally, in the absence of EMI, i.e., when $\tilde{f} = \emptyset$, the individual impact of temperature T on the IC failure due to EMI is considered to be constant with time. From Table 1, it can noted that at extreme temperatures ($T = t_1$ or t_3) the output frequencies are not within the the tolerable limits and vice versa for ambient temperature (t_2). Hence, $P(e|\tilde{f}, t_1) = P(e|\tilde{f}, t_3) = 1.0$ and $P(e|\tilde{f}, t_2) = 0.0$.

As an example of using the noisy-OR CPD function, the probability of EMI failure of RO given $T = t_1$ (−40 °C) due to a two-tone disturbance, $\tilde{f} = \{f_1, f_2\}$, where node variables $\{F_1, F_2\}$ correspond to frequencies {100, 200} MHz respectively is calculated using (2) as:

$$\begin{aligned} P_N(e|\tilde{f}, t_1) &= 1 - \{(1-0) \times (1 - P_M(e|f_1, t_1)) \\ &\quad \times (1 - P_M(e|f_2, t_1))\} = 1 \\ &\quad - \{1 \times (1 - 0.282) \times (1 - 0.951)\} = 0.965 \end{aligned} \quad (3)$$

Further, to calculate the probability of EMI failure due to two-tone disturbance, $\tilde{f} = \{f_1, f_2\}$ in the system environment at a temperature, $T = t_1$, the result of noisy-OR CPD function from (3) and the MPDs of $P(t_1)$, $P(f_i)$ and $P(\bar{f}_j)$ are used in (1) as:

$$\begin{aligned} &P(E = e, F = \tilde{f}, T = t_1) \\ &\quad = P_N(e|\tilde{f}, t_1) \times P(t_1) \times \prod_{f_i\in\tilde{f}} P(f_i) \times \prod_{\bar{f}_j\in\bar{\tilde{f}}} P(\bar{f}_j) \\ &\quad = 0.965 \times 0.1 \times 0.5^2 \times 0.5^8 = 9.423 \times 10^{-5} \end{aligned} \quad (4)$$

where $P(f_i)$, for $i = 1, 2$ and $P(\bar{f}_j)$, for $j = 3$ to 10 are probability of the EM disturbances present and absent in the system environment, respectively. Since, the system environment is unknown, $P(f_i) = P(\bar{f}_j) = 0.5$. Which in addition to the assumption of a low probability for extreme temperature $P(t_1) = 0.1$, has reduced the probability of EMI causing failure in system environment significantly. Similarly, if the CPD value of $P(e|\tilde{f}, t_1)$ is taken from measurements, i.e., if $P_M(e|\tilde{f}, t_1)$ from Table 4, RO at -40 °C for {100, 400}MHz is used in (4), then $P(e, \tilde{f}, t_1)$ further reduces to 8.1112×10^{-5}. Several such probabilistic queries can be answered using the BN shown in Fig. 8. Other deterministic CPD functions that can be used in the BN for more accurate predictions of the multitone failure CPD entries is discussed in Section VI.

C. IDENTIFICATION OF CAUSAL INTERACTIONS

Using the noisy-OR expression given in (2), the probability of IC failure due to two-tone and three-tone EM disturbances that were considered in measurements are calculated with independence assumptions. The probability values obtained using the measurement data, P_M (as previously discussed in Section III. C), and the causal independence assumptions, P_N are provided in Tables 4 and 5 (see Section VI), for some of the two-tone and three-tone examples, respectively. Based on the *degree of synergy*, *DoS* [10], which is calculated by:

$$DoS = 100 \left[\frac{P_M(e|\tilde{f}, T) - P_N(e|\tilde{f}, T)}{P_N(e|f, \tilde{T})} \right] \quad (5)$$

all the multitone disturbances are classified into the three types of causal interactions, namely: *synergy* ($DoS > 0$) and *asynergy* or *inhibition* ($DoS < 0$). Note that for some multitone combinations, e.g., for the two-tone frequencies (in MHz) {100, 200} (CSVCO at 120 °C), the *DoS* is greater than 100 (approximately, 9.99×10^5). This occurs mainly when

either one or more of the single-tones in the multitone combination has no failures, but there is a probability of failure observed from the corresponding multi-tone measurement. For instance, using the previous example of two-tone combination $\{100, 200\}$, $P_M(e|\tilde{f} = \{100\}) = P_M(e|\tilde{f} = \{200\}) = 0.0001$), whereas ($P_M(e|\tilde{f} = \{100, 200\}) = 1.0$). Several other examples of *DoS* greater and less than zero are given in Tables 4 and 5. A detailed discussion on the observed proportion of causal interaction types for two distinct oscillators at different temperatures is described in the next section.

The second main purpose of applying the BN for multitone immunity analysis is for its ability to use deterministic CPD functions to predict the CPD of IC failure even if probability entries of several combinations of multitone disturbances are missing. In Section VI, the verification will be done by estimating the mean prediction error of the noisy-OR, P_N ARNOR, P_A and I-ARNOR, P_I deterministic functions, when compared to the probability of IC failure estimated using measurement P_M.

V. EXPERIMENTAL RESULTS AND DISCUSSION

For injected single-tone EMI frequencies greater than 600 MHz at 10 dBm power level, there were fewer failures for both oscillators at ambient and extreme temperatures. It is deduced that the combined effect of the CQFP package and the capacitance of the input pad results in filtering effects, hence, attenuating the power of higher injected frequencies. Furthermore, for all measurement results, no clamping by the ESD structures in the padring was observed at the output pin. The reason for that is the injected power level of 10 dBm for all single and multitone EM frequencies being insufficient to trigger the ESD structures. For calculation purposes, the absence of failure is considered 0.0001 (shown in Table 3 as 0.0), whereas the certainty of failure is considered 0.999 (shown in Table 3 as 1.0).

Inhibition interactions are less of a concern to the multi-tone EM immunity of an IC due to the cancelling effect of inter-modulations. Conversely, interactions with positive causality, either synergy or asynergy, are significant as they increase the probability of EMI failure. This section describes about the comparison and analysis of the multitone EM immunity of each tested oscillator under the influence of thermal stress.

A. MULTITONE IMMUNITY ANALYSIS AT AMBIENT TEMPERATURE: CSVCO VS. RO

From a risk perspective, interactions between multitone disturbances that are identified as synergistic or asynergistic should be assessed further, especially if multitone disturbance is likely in the intended system environment where the IC is functioning. The interaction types of 29 two-tone and 40 three-tone combinations are displayed for the CSVCO & RO at 25 °C, −40 °C, and 120 °C from Fig. 9 to Fig. 14. Relevant information that need to be considered before analyzing all multitone interaction plots (ambient and extreme temperatures) are as follows:

- For all inhibition interactions, the magnitude of *DoS* is less than or equal to 100.
- The *y*-axis is represented in logarithmic scale in order to highlight the extreme deviations in magnitude of *DoS* caused by synergistic interactions.
- The rise in the number of two and three-tone noise samples corresponds to the increase in the frequency of the EM disturbances.
- The dashed vertical line located in the middle of the plots represents the transition in multitone EMI frequencies from S_1 ([100 MHz - 600 MHz]) to S_2 ([500 MHz - 1 GHz]).

To start with, the CSVCO subjected to two-tone EM disturbances at ambient temperature was analyzed (Fig. 9 (a)). It was noticed that most synergistic interactions occur within S_1 frequency set. The magnitude of *DoS* corresponding to these synergy points is substantially greater than 100, implying that the probability of EMI failure due to two-tone is much higher than the individual single-tone. Moreover, such a very high *DoS* means that the new output frequency is being locked to one of the sub-harmonics of the injected multitone EMI. Inhibition interactions are observed mostly for higher frequency combinations (S_2) with the magnitude of *DoS* close to 100. This indicates that the probability of EMI failure due to two-tone is marginally lower than single tone.

The behavior of causal interactions for three-tone EM disturbance (Fig. 9 (b)) is essentially similar to two-tone except that the number of inhibition interactions have increased in both S_1 & S_2. Moreover, all inhibition noise samples in S_1 have their respective magnitude of *DoS* dropped to 0. This is the result of higher order tones causing a rise in intermodulation effects, hence, eliminating the impact of each other. Consequently, the probability of EMI failure due to higher order disturbances tends to be significantly lower than that of the individual single-tones. No asynergistic interactions were exhibited by the CSVCO at ambient temperature for two and three-tone EM disturbances, meaning that all positive causality interactions are causally dependent.

In contrast, the RO shows a distinct behavior to two and three-tone EM disturbances (Fig. 10 (a) and (b)). All possible multitone interactions (i.e synergy, asynergy & inhibition) were monitored over the entire frequency range (S_1 & S_2). The magnitude of *DoS* for all synergistic interactions is lower by the order of 10^2 when compared to the CSVCO. This conveys that the output frequency is not always locked to the injected two-tone EMI. In contrast to the CSVCO, all of the inhibition interactions for two and three-tone EM disturbances for the RO are close to 100.

Further evaluation of multitone immunity for the RO at ambient temperature shows that, by increasing the number of tones from two to three, the proportion of asynergy type interactions tend to increase for both frequency sets S_1 and S_2. Thus, reducing the inhibition and synergy type interactions. This signifies that the probability of EMI failure rises with the increase in the number of simultaneous disturbances (due to increase in asynergistic proportion). However, approximation

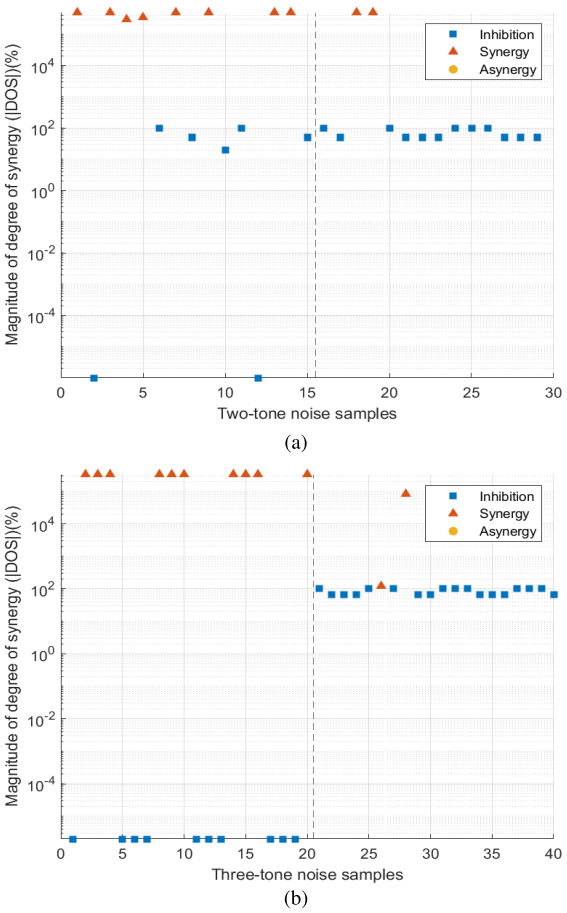

FIGURE 9. Observed causal interactions of CSVCO at ambient temperature: (a) two-tone; (b) three-tone.

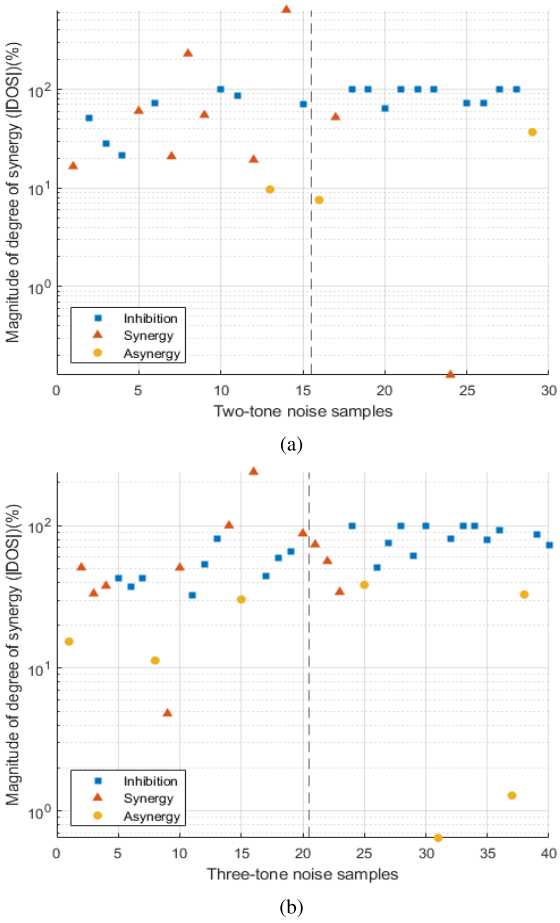

FIGURE 10. Observed causal interactions of RO at ambient temperature: (a) two-tone; (b) three-tone.

in such cases using the noisy-OR model serves as a conservative approach.

B. MULTITONE IMMUNITY ANALYSIS AT EXTREME TEMPERATURES: CSVCO VS. RO

In Section II. C, it was demonstrated that the output frequency of both oscillators was inversely proportional to the surge in temperature whereas the frequency of the CSVCO was more resilient to temperature changes compared to the RO. In this section, the multitone EM immunity of the CSVCO and RO is characterized including the effect of temperature variation.

The interaction types associated to two and three-tone EMI for CSVCO at -40 °C are illustrated in Fig. 11 (a) and (b), respectively. At the minimum temperature, the overall synergistic interactions were increased and shifted to higher frequencies (S_1 to S_2), specifically for three-tone EM disturbances. However, the respective magnitude of *DoS* for synergy points at lower frequencies (S_1) is substantially reduced. The *DoS* for higher frequencies (S_2) has remained unaffected by temperature. Consequently, the inhibition interactions are reduced when increasing the order of tones from two to three with the *DoS* always being greater than 0. These results demonstrate that the CSVCO is truly susceptible to multi-tone EM disturbances at -40 °C. Only one asynergistic point was detected in S_1 for two-tone EMI, implying that the reduction in temperature does not primarily change the type of positive causality for the CSVCO.

When analyzing the effect of multitone EM disturbances on the RO at -40 °C (Fig. 12 (a) & (b)), the inhibition interactions are relatively higher than previously noticed at ambient temperature. Synergistic interactions were less frequent and shifted to higher frequencies S_2. No asynergistic interactions were monitored for all multitone EMI corresponding to the RO at that temperature. In divergence to the CSVCO, the RO was found to be more immune to multitone EM disturbances at -40 °C. Moreover, the asynergistic interactions tend to diminish for the RO with the decrease in temperature. For both oscillators, a shift from low to high frequency for synergistic interactions was observed while lowering the temperature. Since both oscillators have different topology, the observed shift in frequency could be due to the effect of the package, the I/O pad capacitance, and the FD circuit at minimum temperature.

Fig. 13 (a) and (b) represents the causal interactions of the CSVCO at maximum temperature. The number of synergistic interactions was significantly increased in S_1 with the rise in

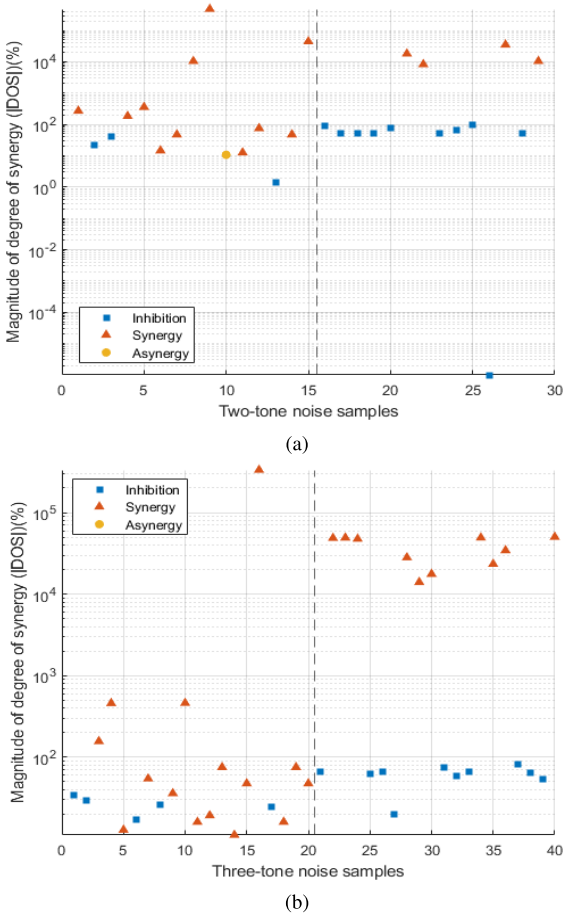

FIGURE 11. Observed causal interactions of CSVCO at −40 °C: (a) two-tone; (b) three-tone.

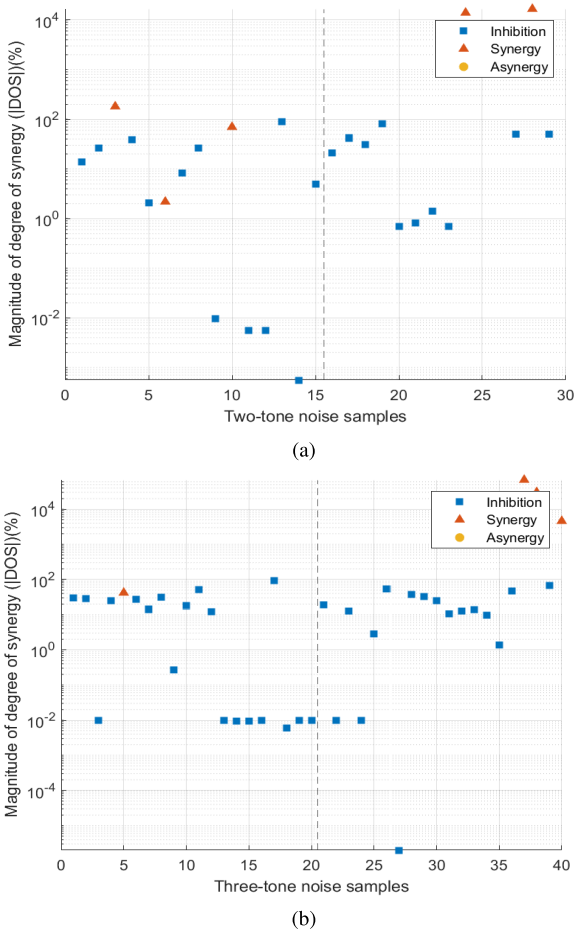

FIGURE 12. Observed causal interactions of RO at −40 °C: (a) two-tone; (b) three-tone.

temperature. Although, the *DoS* for the synergy points has reduced and no shift in frequency is noticed for either two or three-tone EMI. With the increase in number of tones, inhibitions tend to decrease, meaning that inter-modulation effects result in positive causality.

The RO also has more synergistic interactions at the elevated temperature due to two and three-tone EMI as seen in Fig. 14 (a) and (b), respectively. Moreover, the magnitude of *DoS* of synergy points has lowered in S_1 with no visible shift in frequencies. Interestingly, most asynergistic interactions were shifted from S_2 to S_1. For higher EM multitone frequencies (S_2), nearly all interactions are inhibition with a constant *DoS* close to 100. It can be outlined that at maximum temperature the probability of failure due to multitone EMI increases for both oscillators, being more pronounced for the CSVCO. The RO was found to be more immune compared to the CSVCO at 120 °C.

C. COMPARISON OF CAUSAL INTERACTION PROPORTIONS: CSVCO VS. RO

The proportions of causal interaction types for the CSVCO & RO as a result of two and three-tone EM disturbances (nominal and extreme temperatures) are compiled in Fig. 15 (a) and (b), respectively. For two-tone EMI at 25 °C, the inhibition interactions are 6% higher for the CSVCO in comparison to the RO. Furthermore, by observing the positive causality, the RO has 10% higher asynergy interaction points and 4% lower synergy interactions than the CSVCO. That observation shows that the probability of failure due to two-tone EM disturbance at ambient temperature for the RO is slightly lower than the CSVCO due to having a higher overall positive causality.

When evaluating the temperature effect for two-tone EMI on both oscillators (Fig. 15 (a)), the multitone EM immunity of the CSVCO is drastically affected. At −40 °C, the inhibition proportions for the CSVCO were reduced by 20%, while raised by 11% for the RO when compared to ambient temperature. Additionally, at that temperature, the inhibition for the RO was 31% higher than the CSVCO. Unlike the CSVCO where the two-tone EM immunity was deteriorated, the RO had improved immunity at −40 °C.

Compared to ambient temperature, for two-tone EMI at 120 °C, the proportion of inhibition was reduced by 10% and 4% for the CSVCO and RO, respectively. When comparing both oscillators, the synergy interactions of the CSVCO were

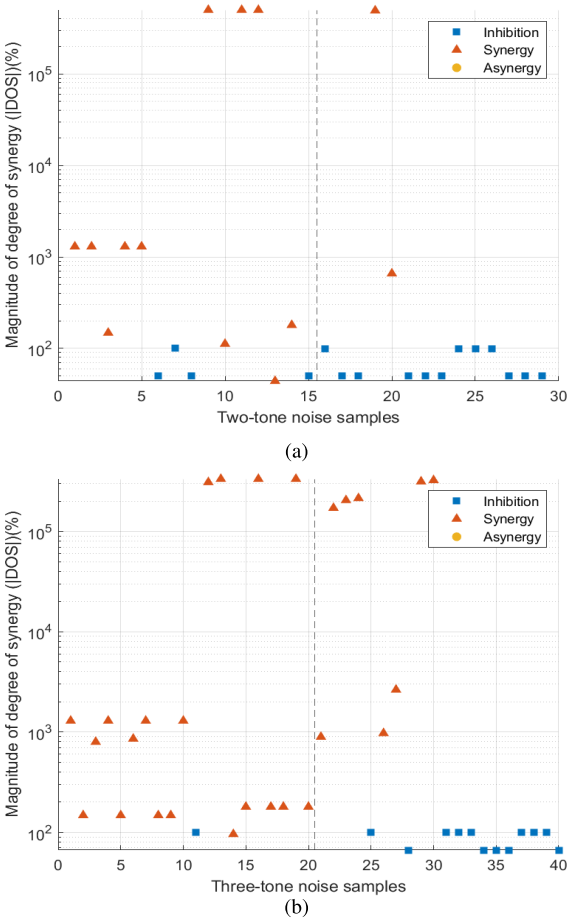

FIGURE 13. Observed causal interactions of CSVCO at 120 °C: (a) two-tone; (b) three-tone.

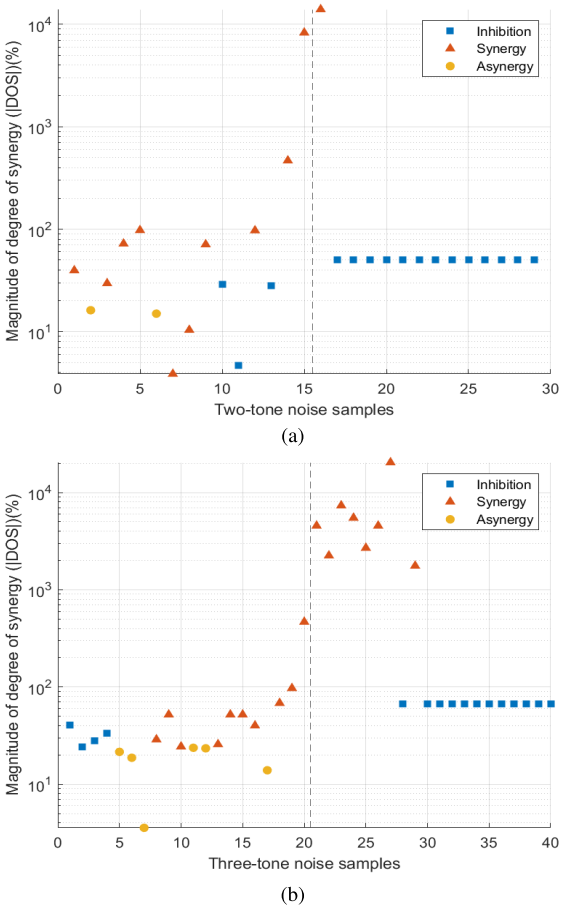

FIGURE 14. Observed causal interactions of RO at 120 °C: (a) two-tone; (b) three-tone.

7% higher than the RO, while their inhibition proportions were equivalent at the highest temperature. Consequently at 120 °C, the probability of failure of the CSVCO was found to be higher to two-tone EMI than the RO.

For three-tone EMI at ambient temperature (Fig. 15 (b)) the proportion of inhibition interactions for the CSVCO was 16% higher than the RO. Additionally, the asynergical points were 18% lower for the CSVCO compared to the RO. At the nominal conditions, the probability of failure for multitone EM disturbance is lower for CSVCO than RO. This is due to the architecture of the CSVCO, as the multitone RF signal initially disturbs the biasing transistors before eventually reaching the inverter stage. When increasing the tones from two to three, the inhibition interactions rise by 5% for the CSVCO whereas it drops by 5% for the RO. For the CSVCO the, inter-modulation frequencies are cancelling each other out leading to inhibition, while they increase the positive causality for the RO.

Similarly to two-tone, for three-tone EMI at extreme temperatures, the CSVCO is more prone to failure. In comparison to ambient temperature, at −40 °C, the synergistic proportions increase considerably by 33% for the CSVCO, while reducing by 18% for the RO. At that temperature, the RO has significantly higher (63%) inhibition points than the CSVCO. Moreover, by raising the temperarure to 120 °C, for three-tone EMI, the synergistic interactions for the RO and CSVCO increase by 17% and 38%, respectively. Nevertheless, the synergistic points of the RO are 23% less than those of the CSVCO at maximum temperature. That clearly suggests that at extreme temperatures the RO is more resilient to multi-tone EMI compared to the CSVCO.

To summarize, the multitone EM immunity of a CSVCO and RO was experimentally compared and analyzed. The differences in the proportion of interaction types between both oscillators demonstrate that the EMI performance can vary depending on their design and architecture. At nominal temperature the CSVCO was found to be less susceptible to two and three-tone EMI than the RO. With the rise in the order of tones, the inter-modulation effects cause an increase in the proportion of inhibition interactions for the CSVCO while raising the positive causality for the RO. At extreme temperatures, the probability of failure for the RO due to multi-tone EMI is lower than the CSVCO. This means that even though the output frequency of the CSVCO was more resilient to temperature changes compared to the RO (see

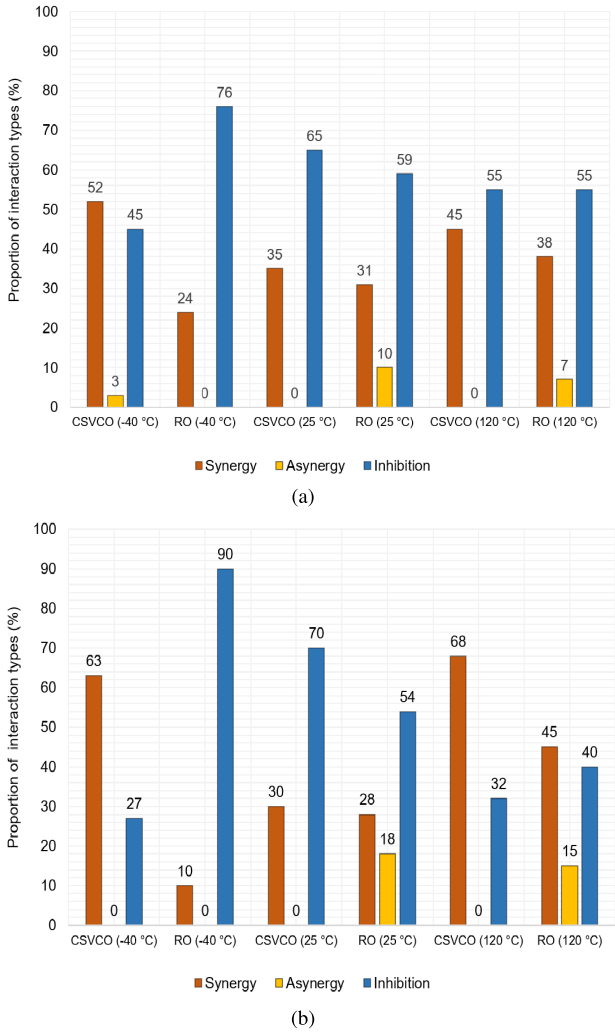

FIGURE 15. Comparison of proportion of interaction types of the CSVCO and RO caused by multitone EM disturbance with the added effect of temperature: (a) two-tone; (b) three-tone.

Section II. C), it is still more susceptible to multitone EM disturbances under thermal stress.

VI. PREDICTION ACCURACY OF DETERMINISTIC CPD FUNCTIONS

The deterministic CPD functions discussed in Section IV to predict the probability of multitone disturbances are verified by comparing the estimated probability values corresponding to the 40 three-tone EM disturbances considered for this study. As the verification is done both for CSVCO and RO at all three temperatures, the generality of the reliability of deterministic CPD functions is also verified.

1) NOISY-OR

Noisy-OR CPD functions are purely based on the causal independence assumptions, and moreover, the expression uses only the failure probabilities of single-tones to predict multitone failure probabilities. Which means, having a low value of prediction error, i.e., $P_M - P_N$ for three-tone disturbances

TABLE 2. Summary of the prediction accuracy of deterministic CPD functions for the IC failures due to three-tone EMI.

IC	Temperature	Method	Mean Prediction Error	Standard Deviation
CSVCO	−40 °C	Noisy-OR	-0.010	0.44
		ARNOR	-0.193	0.29
		I-ARNOR	-0.040	0.17
	25 °C	Noisy-OR	0.192	0.50
		ARNOR	-0.213	0.35
		I-ARNOR	0.019	0.33
	120 °C	Noisy-OR	0.47	0.41
		ARNOR	-0.028	0.22
		I-ARNOR	0.105	0.23
RO	−40 °C	Noisy-OR	-0.137	0.22
		ARNOR	-0.150	0.21
		I-ARNOR	-0.002	0.22
	25 °C	Noisy-OR	-0.100	0.18
		ARNOR	-0.186	0.23
		I-ARNOR	-0.035	0.21
	120 °C	Noisy-OR	0.04	0.22
		ARNOR	-0.092	0.17
		I-ARNOR	-0.075	0.18

will indicate that the independence assumptions are true. However, taking the mean prediction error for all 40 known three-tone disturbances into account, it was observed that the noisy-OR prediction is in general, not very reliable. This is because, for some combinations, e.g., for CSVCO at −40 °C, the independence assumptions are not valid, hence leading to a higher standard deviation of 0.44. At higher temperatures, e.g., for CSVCO at 120 °C, where 68% of the combinations are of the synergistic type, the noisy-OR CPD function underestimates the probability of failure.

2) ARNOR AND I-ARNOR

The expressions of the deterministic functions of ARNOR and I-ARNOR that were used in [10], were modified in this paper to include the temperature effects, and are given in (7) and (8) respectively. Both ARNOR and I-ARNOR are descendants of the noisy-OR model and are based on the recursive-noisy-OR (RNOR) expression given in (6). The deterministic CPD functions of RNOR (P_R), ARNOR (P_A) and I-ARNOR (P_I), including the temperature node variable T, as shown in Fig. 8, are given as:

$$P_R(e|\tilde{f}, T) = \begin{cases} P_M(e|\tilde{f}, T), \\ \text{if available} \\ 1 - \prod_{k=0}^{r-1} \left[\dfrac{1 - P_R(e|\tilde{f}, T \setminus \{c_{k+1}\})}{1 - P_R(e|\tilde{f}, T \setminus \{c_{k+1}, c_{\text{mod }(k+1,r)+1}\})} \right], \\ \text{otherwise} \end{cases} \quad (6)$$

TABLE 3. Probability of the EMI failure of CSVCO and RO due to single-tone disturbances.

Single-tone (MHz)	100	200	300	400	500	600	700	800	900	1000
CSVCO (−40 °C)	0.179	0.0	0.571	0.679	0.0	0.0	1.0	0.0	0.0	0.0
CSVCO (25 °C)	0.0	0.0	1.0	0.0	0.0	0.0	0.329	0.0	0.0	0.0
CSVCO (120 °C)	0.071	0.0	0.0	0.357	0.0	0.0	0.036	0.0	0.0	0.0
RO (−40 °C)	0.282	0.951	0.564	0.056	1.0	1.0	0.0	0.0	0.0	0.0
RO (25 °C)	0.33	0.011	0.606	0.063	0.017	0.059	0.042	0.031	0.092	0.095
RO (120 °C)	0.317	0.585	0.507	0.176	0.0	0.0	0.0	0.0	0.0	0.0

TABLE 4. Probability of the EMI failure due to two-tone disturbances.

Two-tone (MHz)	100 200	100 300	100 500	200 300	200 600	300 500	400 600	500 600	500 800	600 700	600 1000	700 800	800 900	900 1000
CSVCO (−40 °C)														
P_M	0.662	0.507	0.507	0.655	0.965	0.643	1	0.089	0	0.225	0	0.352	0.07	0.021
P_N	0.179	0.648	0.179	0.571	0	0.571	0.679	0	0	1	0	1	0	0
DOS (%)	>100	-21.7	>100	14.6	>100	12.6	47.3	>100	-50	-77.5	-50	-64.8	>100	>100
Causality	S	I	S	S	S	S	S	S	I	I	I	I	S	S
CSVCO (25 °C)														
P_M	1	1	0.6	0	1	0	1	0	0	0	0	0	0	0
P_N	0	1	0	1	0	1	0	0	0	0.329	0	0.329	0	0
DOS (%)	>100	0	>100	-100	>100	-100	>100	-50	-50	-100	-50	-99.97	-49.997	-49.997
Causality	S	I	S	I	S	I	S	I	I	I	I	I	I	I
CSVCO (120 °C)														
P_M	1	1	1	0	1	1	1	0	0	0.271	0	0	0	0
P_N	0.072	0.072	0.072	0	0	0	0.357	0	0	0.036	0	0.036	0	0
DOS (%)	>100	>100	>100	-50	>100	>100	>100	-50	-50	>100	-50	-99.7	-50	-50
Causality	S	S	S	I	S	S	S	I	I	S	I	I	I	I
RO (−40 °C)														
P_M	0.831	0.508	0.617	1	1	1	1	0.951	0.567	0.993	0.993	0.028	0	0
P_N	0.965	0.687	1	0.979	1	1	1	1	1	1	1	0	0	0
DOS (%)	-13.9	-26	-38.3	2.2	0	0	0	-4.9	-43.3	-0.7	-0.7	>100	-50	-50
Causality	I	I	I	S	I	I	I	I	I	I	I	S	I	I
RO (25 °C)														
P_M	0.393	0.357	0.268	0.162	0.107	0.085	0.875	0.021	0.071	0.036	0	0.071	0	0.113
P_N	0.337	0.736	0.341	0.61	0.069	0.612	0.118	0.074	0.047	0.098	0.148	0.071	0.12	0.178
DOS (%)	16.5	-51.5	-21.4	-73.4	54.9	-86.2	>100	-71.6	52.1	-63.6	-99.9	0.1	-99.9	-36.8
Causality	S	I	I	I	S	I	S	I	S	I	I	S	I	A
RO (120 °C)														
P_M	1	0.556	0.546	0.676	1	0.483	1	0.017	0	0	0	0	0	0
P_N	0.716	0.663	0.317	0.795	0.585	0.507	0.176	0	0	0	0	0	0	0
DOS (%)	39.6	-16.2	72.2	-15	71.1	-4.7	>100	>100	-50	-50	-50	-50	-50	-50
Causality	S	A	S	A	S	I	S	S	I	I	I	I	I	I

$$P_A(e|\tilde{f},T) = \begin{cases} P_M(e|\tilde{f},T), \\ \text{if available and, } \tilde{f},T\text{: positive causality} \\ P_N(e|\tilde{f},T), \\ \text{if } P_M(e|\tilde{f},T) \text{ is available and,} \\ \tilde{f},T\text{: inhibition} \\ P_R(e|\tilde{f},T) \\ \text{otherwise} \end{cases} \tag{7}$$

$$P_I(e|\tilde{f},T) = P_R(e|\tilde{f},T)\left[1+\frac{0.01}{m}\sum_{i=1}^{m} DoS_m\right]. \tag{8}$$

The invalidity of RNOR to predict multitone failure probability has already been discussed in [10], hence is not discussed in this paper. Note that, when using the I-ARNOR CPD function given in (8), the weighting parameter DoS_m corresponding to any multitone interaction of type synergy and asynergy is considered as 0.

TABLE 5. Probability of the EMI failure due to three-tone disturbances.

Three-tone (MHz)	100, 200, 300	100, 200, 600	100, 300, 600	100, 500, 600	200, 300, 600	200, 500, 600	300, 500, 600	500, 600, 800	500, 700, 800	500, 800, 900	600, 700, 800	600, 800, 900	700, 800, 900	800, 900, 1000
CSVCO (−40 °C)														
P_M	0.428	0.996	1	1	1	1	1	0.146	0.383	0.085	0.254	0.148	0.182	0.151
P_N	0.648	0.179	0.648	0.179	0.572	0	0.572	0	1	0	1	0	1	0
DOS (%)	-34	>100	54.3	>100	75	>100	75	>100	-61.7	>100	-74.6	>100	-81.8	>100
Causality	I	S	S	S	S	S	S	S	I	S	I	S	I	S
CSVCO (25 °C)														
P_M	1	1	1	1	1	1	1	0	0	0.25	0	0.0	0.0	0.0
P_N	1	0	1	0	1	0	1	0	0.329	0	0.329	0.0	0.329	0.0
DOS (%)	0	>100	0	>100	0	>100	0	-66.7	-100	>100	-100	-66.7	-100	-66.7
Causality	I	S	I	S	I	S	I	I	I	S	I	I	I	I
CSVCO (120 °C)														
P_M	1	1	1	1	1	1	1	0.514	0	0	0	0	0	0
P_N	0.072	0.072	0.072	0.072	0	0	0	0	0.036	0	0.036	0	0.036	0
DOS (%)	>100	>100	>100	>100	>100	>100	>100	>100	-99.7	-66.7	-99.7	-66.7	-99.7	-66.7
Causality	S	S	S	S	S	S	S	S	I	I	I	I	I	I
RO (−40 °C)														
P_M	0.687	0.751	0.858	0.817	1	1	1	1	0.972	0.62	0.894	0.901	0.204	0.014
P_N	0.985	1	1	1	1	1	1	1	1	1	1	1	0	0
DOS (%)	-30.2	-24.9	-14.2	-18.3	0	0	0	0	-2.8	-38	-10.6	-9.9	>100	>100
Causality	I	I	I	I	I	I	I	I	I	I	I	I	S	S
RO (25 °C)														
P_M	0.625	0.518	0.429	0.571	0.125	0.286	0.214	0.161	0.054	0	0.125	0	0.155	0.056
P_N	0.739	0.376	0.751	0.38	0.633	0.085	0.635	0.103	0.087	0.135	0.126	0.172	0.157	0.204
DOS (%)	-15.4	37.7	-42.9	50.6	-80.3	>100	-66.3	56.2	-38.4	-99.9	-0.6	-99.9	-1.3	-72.3
Causality	A	S	I	S	I	S	I	S	A	I	A	I	A	I
RO (120 °C)														
P_M	0.513	0.478	0.64	0.394	1	0.819	1	0.007	0.008	0	0	0	0	0
P_N	0.86	0.716	0.663	0.317	0.795	0.585	0.507	0	0	0	0	0	0	0
DOS (%)	-40.4	-33.3	-3.6	24.4	25.7	40.1	97.2	>100	>100	-66.7	-66.7	-66.7	-66.7	-66.7
Causality	I	I	A	S	S	S	S	S	S	I	I	I	I	I

The mean prediction error and standard deviation values obtained by applying the CPD functions in (7) and (8), for the 40 known three-tone disturbances are summarized in Table 2. In general, lower mean prediction error and standard deviation are observed for I-ARNOR model when compared to the ARNOR and the noisy-OR model. Even for the two exceptional cases where the noisy-OR has a relatively lower mean prediction error than I-ARNOR, i.e., for CSVCO at −40 °C and RO at 120 °C, the respective standard deviation is still relatively higher for the noisy-OR. For almost all cases except (CSVCO at 120 °C) the I-ARNOR has lower mean prediction error and slightly lower or higher standard deviation when compared to the ARNOR model. This implies the significance of using the mean *DoS* [10] for more accurate results. Consequently, this verifies the general prediction capability of the I-ARNOR deterministic CPD function limited to third-tone EMI failure probability. Additional verification of higher-order multitone EM disturbances is however considered for future work.

To illustrate the possible frequency combinations, the associated probability of failures, the *DoS*, and the interaction proportions (i.e. synergy (S), asynergy (A), and inhibition (I)) of the CSVCO & RO at −40 °C, 25 °C, and 120 °C are included in Tables 3, 4, & 5 for single-tone, two-tone and three-tone EM disturbances, respectively.

VII. CONCLUSION

The conducted immunity of two SOI integrated oscillators, i.e. CSVCO & RO, was studied when exposed to multitone EM disturbances and temperature variations. The analysis reveals that positive causality (mainly due to synergy or causal dependence) can increase the probability of circuit failure in comparison to single-tone EMI. A generalized multitone EM immunity measurement procedure was also proposed for checking different combinations of multitone frequencies and power levels. By considering the output frequency as the failure criterion all possible causal interactions (i.e inhibition, asynergy, and synergy) were monitored for the studied oscillators, varying the probability of failure due to multitone EMI.

At ambient temperature (25 °C), the performance of the CSVCO was found to outperform the RO due to the slightly higher proportions of inhibition for both two and three-tone EM disturbances. Most of the synergistic interactions result from the output frequencies being locked to one of the injected multitone EM disturbances, particularly for the CSVCO. With the rise in the number of tones, the effect of inter-modulation resulted in the increase of the proportion of inhibition for the CSVCO, and of asynergy for the RO. Asynergistic points were mostly observed for the RO over the entire tested frequency spectrum. Moreover, most of the positive causality interactions for both oscillators was observed for multitone combinations with frequencies in range 100 MHz to 600 MHz, which is due to the combined effect of the package, the input pad capacitance, and the FD circuit filtering out the higher multitone frequencies.

Another environmental factor, i.e. temperature variation, indicated a deviation in the output frequency of both oscillators, with the CSVCO being more robust compared to the RO. However, the results were completely reversed when the effects of multi-tone EMI and temperature were combined. The CSVCO was substantially more susceptible to multitone EMI than the RO at extreme temperatures (−40 °C and 120 °C). While taking into account temperature, the probability of EM failure was found to be the lowest for the the inhibition type interactions. The variation in temperature impacted in the transition of synergistic frequency combinations to greater than 600 MHz for both oscillators, especially at the minimum temperature. That verified that temperature had a significant influence on the package, the I/O pad capacitance and the FD circuit of the IC.

As demonstrated in this paper for a simple example, the application of a BN model to include the uncertainties associated to the occurrence of the EM disturbances and other environmental factor(s) such as the temperature, can facilitate an expert to determine the risk of IC or component failure due to EMI in the system environment.

In addition, noisy-OR, ARNOR, and I-ARNOR (introduced in [10]) CPD functions were applied to the considered temperatures to predict the probability of failure due to three-tone EM disturbances for the CSVCO and RO. By comparing the obtained measurement results, it was verified that I-ARNOR was the most accurate at most occasions with a minimal mean prediction error and standard deviation. The use of such deterministic functions will complement and enhance the current EMC standards that includes multitone immunity testing solely aimed at reducing the dwell time, by enabling the prediction of multitone causal interaction types and the estimation of the IC immunity levels for untested combinations of multitone disturbances. This paper emphasizes that by combining probabilistic models and measurement techniques, multitone EM testing can be involved in the conventional DPI, to more precisely characterize the conducted immunity of a circuit at the IC level.

REFERENCES

[1] Y. Zhuang and D. Chen, "Accurate spectral testing with impure test stimulus for multi-tone test," in *Proc. IEEE Int. Test Conf. Asia (ITC-Asia)*, Aug. 2018, pp. 97–102.

[2] J. Li, S. Ma, Q. Liu, Z. Gong, H. Tian, and S. Jin, "Analysis of interference caused by intermodulation in multi-tone radiated immunity tests," in *Proc. IEEE Int. Symp. Electromagn. Compat., IEEE Asia–Pacific Symp. Electromagn. Compat. (EMC/APEMC)*, May 2018, pp. 660–663.

[3] M. Koohestani, M. Ramdani, P. Besnier, J.-L. Levant, and R. Perdriau, "Perturbations of electric and magnetic fields due to the presence of materials in TEM cells," *IEEE Trans. Electromagn. Compat.*, vol. 62, no. 4, pp. 997–1006, Aug. 2020.

[4] *Integrated Circuits—Measurement of Electromagnetic Immunity 150 kHz to 1 GHz—Part 4: Direct RF Power Injection Method*, 1st ed., document IEC 62132-4, 2006.

[5] F. Fiori and M. B. Aimonetto, "Measurement of the susceptibility to EMI of ICs with two-tone interference," in *Proc. IEEE Int. Symp. Electromagn. Compat., IEEE Asia–Pacific Symp. Electromagn. Compat. (EMC/APEMC)*, May 2018, pp. 292–296.

[6] K. Harima, D. Akita, and T. Nakamura, "Investigation of radiated immunity testing using white Gaussian noise and multitone signals," in *Proc. Asia–Pacific Microw. Conf. (APMC)*, Nov. 2018, pp. 782–784.

[7] *Electromagnetic compatibility (EMC)—Part 4–3: Testing and Measurement Techniques—Radiated, Radio-Frequency, Electromagnetic Field Immunity Test*, 4th ed., document IEC 61000-4-3, 2020.

[8] A. Biondi, H. Rogier, D. Vande Ginste, and D. De Zutter, "Multi-tone EMC testing strategy for RF-devices," in *Proc. IEEE Electr. Design Adv. Packag. Syst. Symp. (EDAPS)*, Dec. 2012, pp. 89–92.

[9] J. Pearl, "Belief updating by network propagation," in *Probabilistic Reasoning in Intelligent Systems*. San Francisco, CA, USA: Morgan Kaufmann, 1988, ch. 4, pp. 143–237. [Online]. Available: https://www.sciencedirect.com/science/article/pii/B9780080514895500102

[10] L. Devaraj, Q. M. Khan, A. Ruddle, A. Duffy, R. Perdriau, and M. Koohestani, "Application of probabilistic models for multi-tone electromagnetic immunity analysis," *IEEE Trans. Electromagn. Compat.*, to be published.

[11] Q. M. Khan, L. Devaraj, M. Koohestani, A. Ruddle, M. Ramdani, and R. Perdriau, "Synergistic effect of multitone EMI on the conducted immunity of integrated oscillators," *IEEE Lett. Electromagn. Compat. Pract. Appl.*, early access, May 17, 2022, doi: 10.1109/LEMCPA.2022.3175433.

[12] T. Hino and H. Watanabe, "Analysis of RF noise in LDO and establishment of noise immunity," in *Proc. Int. Symp. Electromagn. Compat. (EMC Europe)*, Sep. 2019, pp. 508–512.

[13] M. Magerl, C. Stockreiter, and A. Baric, "Influence of RF disturbance phase on amplifier DPI characteristics," in *Proc. Int. Symp. Electromagn. Compat. (EMC Europe)*, Sep. 2017, pp. 1–5.

[14] J. Wu, H. Zhang, H. Wang, L. Zheng, H. Ma, and B. Li, "DPI immunity of bandgap in Si and SOI technologies," in *Proc. 11th Int. Workshop Electromagn. Compat. Integr. Circuits (EMCCompo)*, Jul. 2017, pp. 197–199.

[15] S.-Y. Yuan, Y.-L. Wu, R. Perdriau, S.-S. Liao, and H.-P. Ho, "Electromagnetic interference analysis using an embedded phase-lock loop," in *Proc. Asia–Pacific Symp. Electromagn. Compat.*, 2012, pp. 189–192.

[16] A. Lavarda and B. Deutschmann, "Direct power injection (DPI) simulation framework and postprocessing," in *Proc. IEEE Int. Symp. Electromagn. Compat. (EMC)*, Aug. 2015, pp. 1248–1253.

[17] S. O. Land, M. Ramdani, and R. Perdriau, "Dominant coupling mechanism for integrated circuit immunity of SOIC packages up to 10 GHz," *IEEE Trans. Electromagn. Compat.*, vol. 60, no. 4, pp. 965–970, Aug. 2018.

[18] A. Ayed, T. Dubois, J. Levant, and G. Duchamp, "Immunity measurement and modeling of an ADC embedded in a microcontroller using RFIP technique," *IEEE Trans. Electromagn. Compat.*, vol. 57, no. 5, pp. 955–962, Oct. 2015.

[19] H. Pues and C. Gazda, "A black-box measurement-based modeling method for the RF emission and immunity behavior of ICs," in *Proc. IEEE Int. Symp. Electromagn. Compat. (EMC)*, Aug. 2015, pp. 1002–1006.

[20] J. Cheng, C. Zhou, D. Yu, Z. Xu, and D. Zhang, "An ICIM-CI-T model for EMI prediction of IO element on typical FPGA With temperature effect considered," *IEEE Trans. Electromagn. Compat.*, vol. 62, no. 3, pp. 755–764, Jun. 2020.

[21] D. Pommerenke, "Methods for speeding up radiated and conducted immunity tests," in *Proc. IEEE Int. Symp. Electromagn. Compat.*, vol. 2, Aug. 2000, pp. 587–592.
[22] G. Barth, "Benefits of multitone EMC immunity testing," *Int. J. RF Microw. Comput.-Aided Eng.*, vol. 26, pp. 355–358, 2016.
[23] A. Biondi, L. Vallozzi, H. Rogier, D. De Zutter, and F. Declercq, "Electromagnetic compatibility aware design and testing of intermodulation distortion under multiple co-located sources illumination," *IET Sci., Meas. Technol.*, vol. 6, no. 2, pp. 105–112, Mar. 2012.
[24] L. Fu, Z. Yan, C. Fu, and D. Su, "Extraction and analysis of conducted electromagnetic susceptibility elements of integrated circuits," *IEEE Access*, vol. 9, pp. 149125–149136, 2021.
[25] I. P. Tolic, J. Mikulic, G. Schatzberger, and A. Baric, "Design of CMOS temperature sensors based on ring oscillators in 180-nm and 110-nm technology," in *Proc. 43rd Int. Conv. Inf., Commun. Electron. Technol. (MIPRO)*, Sep. 2020, pp. 104–108.
[26] R. A. WaIunj, S. D. Pable, and G. K. Kharate, "Design of robust ultra-low power CMOS voltage controlled ring oscillator with enhanced performance," in *Proc. Int. Conf. Adv. Commun. Comput. Technol. (ICACCT)*, Feb. 2018, pp. 235–239.
[27] J. F. Lemmer and D. E. Gossink, "Recursive noisy OR—A rule for estimating complex probabilistic interactions," *IEEE Trans. Syst., Man, Cybern. B, Cybern.*, vol. 34, no. 6, pp. 2252–2261, Dec. 2004.
[28] M. Mardiguian, "An empirical validation of recursive noisy OR (RNOR) rule for asthma prediction," in *Proc. AMIA Ann. Symp.*, 2010, pp. 16–20.
[29] Q. M. Khan, A. Ramezani, M. Koohestani, M. Ramdani, and R. Perdriau, "A comparison among DPI immunities of multi-stage CSVCOs and ring oscillators," in *Proc. 13th Int. Workshop Electromagn. Compat. Integr. Circuits (EMC Compo)*, Mar. 2022, pp. 123–127.
[30] Q. Mashaal Khan, R. Perdriau, M. Ramdani, and M. Koohestani, "A comparative study of on-chip CMOS S&H voltage sensors for power integrity: SOI vs. bulk," in *Proc. IEEE Int. Joint EMC/SI/PI EMC Eur. Symp.*, Jul. 2021, pp. 911–916.
[31] B. Razavi, "Oscillators," in *Design of Analog CMOS Integrated Circuits*. New York, NY, USA: McGraw-Hill, ch. 15, 2001.
[32] G. De Vita, F. Marraccini, and G. Iannaccone, "Low-voltage low-power CMOS oscillator with low temperature and process sensitivity," in *Proc. IEEE Int. Symp. Circuits Syst.*, May 2007, pp. 2152–2155.
[33] H. Pues and D. Pissoort, "Design of IEC 62132-4 compliant DPI test boards that work up to 2 GHz," in *Proc. Int. Symp. Electromagn. Compat. (EMC Europe)*, Sep. 2012, pp. 1–4.
[34] M. Koohestani, N. Pires, A. K. Skrivervik, and A. A. Moreira, "Bandwidth enhancement of a wearable UWB antenna near a human arm," *Microw. Opt. Technol. Lett.*, vol. 55, no. 12, pp. 2965–2967, Dec. 2013.
[35] M. Koohestani, A. A. Moreira, and A. K. Skrivervik, "Feeding structure influence on performance of two UWB antennas near a human arm," in *Proc. 8th Eur. Conf. Antennas Propag. (EuCAP)*, Apr. 2014, pp. 834–836.
[36] N. Baptistat, K. Abouda, G. Duchamp, and T. Dubois, "Effects of process-voltage-temperature (PVT) variations on low-side MOSFET circuit conducted emission," in *Proc. 12th Int. Workshop Electromagn. Compat. Integr. Circuits (EMC Compo)*, Oct. 2019, pp. 213–215.
[37] Q. M. Khan, R. Perdriau, M. Ramdani, and M. Koohestani, "A comparative performance analysis of 6T & 9T SRAM integrated circuits: SOI vs. bulk," *IEEE Lett. Electromagn. Compat. Pract. Appl.*, vol. 4, no. 2, pp. 25–30, Jun. 2022.
[38] A. Boyer, B. Li, S. B. Dhia, C. Lemoine, and B. Vrignon, "Construction and evaluation of the susceptibility model of an integrated phase-locked loop," in *Proc. 8th Int. Workshop Electromagn. Compat. Integr. Circuits (EMC Compo)*, 2011, pp. 7–12.
[39] P. Baros, P. Horsky, and P. Kamenicky, "Introduction to EMC simulations of analog ICs," in *Proc. Int. Symp. Electromagn. Compat. (EMC Europe)*, Sep. 2008, pp. 1–6.
[40] J. Hwang, Y. Han, H. Park, W. Nah, and S. Kim, "Radiated electromagnetic immunity analysis of VCO using IC stripline method," in *Proc. 10th Int. Workshop Electromagn. Compat. Integr. Circuits (EMC Compo)*, Nov. 2015, pp. 147–151.
[41] D. Koller and N. Friedman, *Probabilistic Graphical Models: Principles and Techniques* (Adaptive Computation and Machine Learning). Cambridge, MA, USA: MIT Press, 2009.

QAZI MASHAAL KHAN (Graduate Student Member, IEEE) received the bachelor's degree *(summa cum laude)* in electrical engineering from FAST NUCES University, Pakistan, in 2016, and the Joint master's degree (Hons.) in smart systems integration, in 2019. He is currently pursuing the Ph.D. degree with the Radio and Hyper-Frequency (RF) and the Electromagnetic Compatibility (EMC) Group, ESEO, France. This was an EU funded Erasmus+Program, where he spent his four semesters in U.K., Norway, Hungary, and Germany. The host was Heriot-Watt University, U.K. As part of the MSCA ETN PETER, he will carry out the extension of the IC Immunity and Emission models to incorporate environmental stresses. His Doctoral degree will be provided by INSA Rennes University. His research interests include ageing, thermal stresses, and obsolescence on EMC behavior on many categories of ICs.

LOKESH DEVARAJ (Student Member, IEEE) received the B.E. degree in electronics and communication engineering from Anna University, Chennai, India, in 2017, and the M.Sc. degree in advanced optical technologies from Freidrich Alexander University, Erlangen, Germany, in 2019. He is currently pursuing the Ph.D. degree with De Montfort University, Leicester, U.K. As a part of the MSCA ETN PETER, he will carry out research on the Risk–Based Automotive Electromagnetic Engineering Approach aligned with the ISO 26262 Functional Safety Approach. Since 2019, he has been working as an Automotive Electronic Research Engineer with the Department of Vehicle Resilience, HORIBA MIRA Ltd., Nuneaton, U.K. His research interests include risk-based EMC, functional safety, cybersecurity, and statistical models.

RICHARD PERDRIAU (Senior Member, IEEE) was born in Angers, France, in 1971. He received the degree in electronics and computer science engineering from the ESEO Angers-Grande Ecole d'Ingénieurs Généralistes, Angers, in 1992, the Ph.D. degree in applied sciences from the Université Catholique de Louvain, Louvain-la-Neuve, Belgium, in 2004, and the "Habilitation à Diriger des Recherches" (Accreditation degree) from the Université de Rennes 1, Rennes, France, in 2012.

From 1992 to 2012, he was an Associate Professor with the ESEO School of Engineering in the fields of microelectronics and embedded systems. In 2013, he became a Full Professor. His research interests include EMC of integrated circuits, mixed-signal hardware description languages, and integrated circuit design. He served as the Vice-Chair and the Technical Program Co-Chair for EMC Europe 2017. In January 2020, he was elected as the Secretary of the IEEE France Section.

ALASTAIR R. RUDDLE (Senior Member, IEEE) received the B.Sc. degree in physics from the University of Bristol, Bristol, U.K. and the Ph.D. degree in electronic and electrical engineering from the University of Loughborough, Loughborough, U.K.

Since 1996, he has been with HORIBA MIRA Ltd., Nuneaton, U.K., an automotive research and technology organization. He is currently the Chief Scientist for Vehicle Resilience Technologies. Prior to joining HORIBA MIRA Ltd., he carried out research in a number of disciplines in the defense and power industries. He has authored/coauthored more than 160 publications, including articles published in journals and presented at international symposia as well as book chapters. His research interests include computational electromagnetics, electromagnetic measurements, human exposure to electromagnetic fields, and cybersecurity.

Dr. Ruddle is registered as a Chartered Physicist and a Chartered Engineer in the U.K., and participates in a number of international standards activities relating to human exposure to electromagnetic fields and CEM validation.

TIM CLAEYS (Member, IEEE) was born in 1990. He received the M.S. degree in industrial engineering sciences, option electronics from the University College Katholieke Hogeschool Sint-Lieven Gent, Ghent, Belgium, in 2013, and the Ph.D. degree in electrical engineering from KU Leuven, Leuven, Belgium, in 2018.

Since 2018, he has been a Postdoctoral Researcher with the M-Group Research Group (Laboratory FMEC), KU Leuven. His current research interests include near-field scanning, the development of characterization methods for shielding materials and gaskets, electromagnetic interference resilience of wireless protocols, and global reliability of electronic systems.

Dr. Claeys is a part of the IEEE EMC Society Benelux chapter.

MOHAMED RAMDANI (Senior Member, IEEE) received the Ph.D. degree in microelectronics from Université Paul Sabatier, Toulouse, France, in 1989, and the "Habilitation á Diriger des Recherches" (Accreditation degree) from the Université de Rennes 1, Rennes, France, in 2004.

From 1991 to 2008, he was an Associate Professor with ESEO, Angers, France, in the fields of microelectronics and microwave electronics. In 2008, he was promoted to a Full Professor. He has authored several book chapters and many peer-reviewed scientific articles. His research interests include electromagnetic compatibility (EMC) of integrated circuits and integrated circuit design.

Dr. Ramdani is a member of Union Technique de l'Electricité et de la Communication (UTE—French section of the IEC). He served as the General Chair for EMC Europe 2017, which was held in Angers. He was the elected Vice-Chair of the IEEE France Section, in 2016.

MOHSEN KOOHESTANI (Senior Member, IEEE) received the Ph.D. degree (Hons.) in electromagnetics from the école polytechnique fédérale de Lausanne (EPFL), Lausanne, Switzerland, and the Universidade de Lisboa (ULISBOA), Lisbon, Portugal, in 2014.

From 2014 to 2018, he was a Senior Research Fellow with the Institut d'Electronique et de Télécommunications de Rennes (IETR), University of Rennes 1, working mainly on biomedical applications of wireless power transfer systems. He has been an Associate Professor at the ESEO School of Engineering, Angers, France, since 2018. He is also an Associate Researcher at IETR, UMR CNRS 6164. He has authored over 60 peer-reviewed scientific articles. His main research interests include domain of antennas, microwaves, EMC, and biomedical engineering.

Dr. Koohestani is an Official Member of the IEC standardization working group (WG2 and WG9) in the SC47A French subcommittee on the EMC for integrated circuits.